Regioselectively Controlled Synthesis of Colloidal Mushroom Nanostructures and Their Hollow Derivatives

ARTICLE *in* JOURNAL OF THE AMERICAN CHEMICAL SOCIETY · MAY 2010

Impact Factor: 12.11 · DOI: 10.1021/ja101270r · Source: PubMed

4 AUTHORS, INCLUDING:

Claudia Weidenthaler
Max- Planck -Institut für Kohlenforschung, …
133 PUBLICATIONS **2,653** CITATIONS
SEE PROFILE

An-Hui Lu
Dalian University of Technology
133 PUBLICATIONS **7,841** CITATIONS
SEE PROFILE

J|A|C|S ARTICLES

Published on Web 04/26/2010

Regioselectively Controlled Synthesis of Colloidal Mushroom Nanostructures and Their Hollow Derivatives

Mathias Feyen,[†] Claudia Weidenthaler,[†] Ferdi Schüth,[†] and An-Hui Lu*[,‡]

Max-Planck-Institut für Kohlenforschung, Kaiser-Wilhelm-Platz 1, D-45470 Mülheim an der Ruhr, Germany, and State Key Laboratory of Fine Chemicals, School of Chemical Engineering, Dalian University of Technology, Dalian 116012, People's Republic of China

Received February 11, 2010; E-mail: anhuilu@dlut.edu.cn

Abstract: In this study, a facile and controllable synthetic route for the fabrication of mushroom nanostructures (Fe_xO_y@PSD−SiO_2) and their hollow derivatives has been established. The synthesis consists of partial coating of Fe_xO_y (Fe_3O_4 or Fe_2O_3) with polymer spheres, followed by attaching silica hemispheres. The surface-accessible Fe_xO_y nanoparticles on the Janus-type Fe_xO_y@PSD nanospheres are key for directing the growth of the silica hemisphere on the Fe_xO_y@PSD seeds. The size and the porosity of the silica hemispheres are tunable by adjusting the amount of TEOS used and addition of a proper surfactant in a Stöber-type process. After the iron oxide cores were leached out with concentrated HCl, mushroom nanostructures with hollow interiors were obtained, where the morphology of the hollow interior faithfully replicates the shape of the iron oxide core previously filling this void. This synthetic strategy provides a controllable method for the large-scale preparation of asymmetric colloidal nanostructures which could serve as building blocks for the assembly of new types of nanostructures.

1. Introduction

Colloidal nanoparticles are considered as attractive building blocks to create complex materials which have potential applications in the fields of chemistry, applied optics, biology, sensoring, and catalysis.[1] It is obvious that the synthesis of size and morphology controllable colloidal particles is a prerequisite for mastering their chemical and physical properties. Most of the published studies are related to the fabrication of core−shell colloidal particles which are accessible by encapsulation methods: e.g., silica-encapsulated iron oxide,[2−7] silica-encapsulated polystyrene,[8−11] polystyrene-encapsulated silica,[12−14] and many other systems. Recently, the synthesis of colloidal Janus-type particles with specific asymmetric nanostructures or dual-surface functionality has moved into the center of attention, since such systems are valuable in the creation of nano-objects with anisotropic interactions which could lead to the formation of complex structures.[15] The major challenge in this field is the discovery of easy and reproducible synthetic approaches to fabricate Janus nanoparticles, to tailor their properties on the nanoscale, and thus to control their behavior at will. Up to now, a number of techniques have been developed for the synthesis of asymmetric nanoparticles.[16] For example, Janus micelles can be prepared from ABC triblock copolymers that can self-assemble into spherical supermicelles.[17−19] Amphiphilic polymeric Janus particles can be prepared by a microfluidic flow system,[20] biphasic electrofield jetting of two polymer precursors,[21] blend compatibilization of two polymers in a twin-screw mini-mixer,[22] and replication of particle monolayers at liquid surfaces using a gel trapping technique.[23]

[†] Max-Planck-Institut für Kohlenforschung.
[‡] Dalian University of Technology.

(1) Caruso, F. *Colloids and Colloid Assemblies*; Wiley-VCH: Weinheim, Germany, 2004.
(2) Mornet, S.; Grasset, F.; Portier, J.; Duguet, E. *Eur. Cells. Mater.* **2002**, *3* (2), 110.
(3) Lu, Y.; Yin, Y.; Mayers, B. T.; Xia, Y. *Nano Lett.* **2002**, *2*, 183.
(4) Zhao, W.; Gu, J.; Zhang, L.; Chen, H.; Shi, J. *J. Am. Chem. Soc.* **2005**, *127*, 8916.
(5) Lee, J.; Lee, Y.; Youn, J. K.; Bin Na, H.; Yu, T.; Kim, H.; Lee, S.-M.; Koo, Y.-M.; Kwak, J. H.; Park, H. G.; Chang, H. N.; Hwang, M.; Park, J.-G.; Kim, J.; Hyeon, T. *Small* **2008**, *4*, 143.
(6) Deng, Y.; Qi, D.; Deng, C.; Zhang, X.; Zhao, D. *J. Am. Chem. Soc.* **2008**, *130*, 28.
(7) Yi, D. K.; Lee, S. S.; Papaefthymiou, G. C.; Ying, J. Y. *Chem. Mater.* **2006**, *18*, 614.
(8) Tissot, I.; Novat, C.; Lefebvre, F.; Bourgeat-Lami, E. *Macromolecules* **2001**, *34*, 5737.
(9) Lu, Y.; McLellan, J.; Xia, Y. *Langmuir* **2004**, *20*, 3464.
(10) Chen, M.; Wu, L.; Zhou, S.; You, B. *Adv. Mater.* **2006**, *18*, 801.
(11) Graf, C.; Vossen, D. L.; Imhof, A.; Blaaderen, A. V. *Langmuir* **2003**, *19*, 6693.
(12) Corcos, F.; Bourgeat-Lami, E.; Lang, J. *J. Colloid Interface Sci.* **1999**, *210*, 281.
(13) Bourgeat-Lami, E.; Novat, C.; Lang, J. *J. Colloid Polym. Sci.* **1999**, *277*, 1142.
(14) Zhang, S.-W.; Zhou, S.-X.; Weng, Y.-M.; Wu, L.-M. *Langmuir* **2005**, *21*, 2124.
(15) Sun, Q.; Wang, Q.; Jena, P.; Kawazoe, Y. *ACS Nano* **2008**, *2*, 341.
(16) Perro, A.; Reculusa, S.; Ravaine, S.; Bourgeat-Lami, E.; Duguet, E. *J. Mater. Chem.* **2005**, *15*, 3745.
(17) Erhardt, R.; Zhang, M.; Böker, A.; Zettl, H.; Abetz, C.; Frederik, P.; Krausch, G.; Abetz, V.; Müller, A. H. *J. Am. Chem. Soc.* **2003**, *125*, 3260.
(18) Erhardt, R; Boeker, A.; Zettl, H.; Kaya, H.; Pyckhout-Hintzen, W.; Krausch, G.; Abetz, V.; Mueller, A. H. *Macromolecules* **2001**, *34*, 1069.
(19) Erhardt, R.; Boeker, A.; Zettl, H.; Kaya, H.; Pyskhout-Hintzen, W.; Krausch, G.; Abetz, V.; Mueller, A. H. *Polym. Mater. Sci. Eng.* **2001**, *84*, 102.
(20) Nisisako, T.; Torii, T.; Takahashi, T.; Takizawa, Y. *Adv. Mater.* **2006**, *18*, 1152.
(21) Roh, K.-H.; Martin, D. C.; Lahann, J. *Nat. Mater.* **2005**, *4*, 759.
(22) Walther, A.; Matussek, K.; Mueller, A. H. *ACS Nano* **2008**, *2*, 1167.
(23) Paunov, V. N.; Cayer, O. J. *Adv. Mater.* **2004**, *16*, 788.

Microcontact printing was used to prepare asymmetrically coated Janus particles.[24] For example, by printing a PDMS stamp with a suitable ionic surfactant film on latex particle monolayers of opposite surface charge, spherical latex particles with dipolar surface charge distribution were prepared. Further, when the particle monolayer was stamped with another colloid monolayer of different particle size, more complex nanostructures such as half-coated "raspberry"-like particles and doublet particles could be fabricated.

Probably the most frequently used method for the preparation of Janus nanoparticles is the partial surface functionalization of the preprepared nanoparticles, by masking, protecting, or trapping the particle by a medium, so that only the exposed surface is available for chemical modification.[25] The Pickering emulsion approach is often used for the synthesis of Janus particles.[26] This approach is based on the stabilization of wax-in-water emulsions by the colloidal particles, to form the so-called Pickering emulsions.[27] For example, Janus silica particles with sizes varying from 100 to 800 nm, which were decorated with gold colloidal particles, have been prepared from Pickering emulsion.[28] Silica nanoparticles were asymmetrically decorated by gold nanoclusters at a gas−liquid interface.[29] Each hemisphere of these nanostructures can be further specifically functionalized, leading to promising nanomaterials with interesting properties. By a Langmuir interfacial engineering method, amphiphilic gold nanoparticles with dual surfaces have been created:[30] hydrophobic alkanethiolate-protected gold particles dispersed on a water surface were mechanically compressed to partially contact the water phase where hydrophilic thiol derivatives had previously been injected. After ligand exchange in the water subphase, Janus gold nanoparticles were obtained.

Janus silica nanoparticles, regioselectively functionalized by two different chemical groups, were synthesized through a multistep procedure based on the use of a polystyrene nodule as a protecting mask.[31] Raspberry-like hybrid polystyrene−silica nanostructures were prepared by using polymerizable surface group modified silica spheres as seeds for the emulsion polymerization of styrene.[32] When the number ratio between the silica seeds and the growing nodules was kept close to 1, snowman-like or dumbbell-like hybrid nanostructures were produced.[33]

Magnetic Janus nanoparticles (5 or 20 nm in size) are interesting because of their magnetism and dual surface character.[34,35] For example, magnetic Janus nanoparticles have been synthesized which consist of ~5 nm magnetite nanoparticles coated on one side with a pH-dependent and temperature-independent poly(acrylic acid) and functionalized on the other side by a second polymer that is either a pH-independent polymer (polystyrene sodium sulfonate) or a temperature-dependent polymer (poly(*N*-isopropyl acrylamide).[28] Recently, a flame synthetic approach was developed for the preparation of spherical magnetic Janus nanoparticles consisting of γ-Fe_2O_3 and silica.[36] However, the size distribution of this kind of particle is quite polydisperse, from 40 to 200 nm.

After a thorough survey of the literature, a general theme in most of the reports is modification or decoration of part of the surfaces of the particles by masking methods. Only a few publications have dealt with the fabrication of spatially asymmetric particles consisting of organic and inorganic blocks with particle sizes smaller than 100 nm, and magnetic functionality and porosity have rarely been addressed. Hence, there is still a need for the development of simple pathways directly from solution to result in the controlled formation of colloidal particles with complex structures.

In the following, we demonstrate a method for the synthesis of asymmetric nanostructures, mushroom-type nanostructures consisting of iron oxide, poly(styrene-*co*-divinylbenzene) (PSD), and (mesostructured) silica. Iron oxide nanoparticles were first immobilized in PSD nanospheres, which then act as anchor sites for regioselective growth of silica hemispheres. These types of nanostructures can be easily converted to hollow derivatives after removal of the immobilized iron oxide cores with acid.

2. Experimental Section

2.1. Chemicals. Ammonium peroxodisulfate (≥98.0%), ammonium hydroxide solution (28 wt %) in water, and iron(II) chloride tetrahydrate (≥99.0%) were purchased from Fluka. 16-Heptadecenoic acid (HDA) was prepared by following the synthesis of Mirviss et al.[37] The final product was received with a purity of 96% analyzed by ESI-MS. Iron(III) chloride hexahydrate (≥99%), divinylbenzene (technical grade, 80% mixture of isomers), L-lysine (>99.0%), tetrabutylammonium bromide (TBABr, 99%), cetyltrimethylammonium bromide (CTABr, 98%), polyvinylpyrrolidone K 90 (PVP-90), and tetraethyl orthosilicate (TEOS) (98.0%) were obtained from Sigma Aldrich, while glycidyl methacrylate (≥95%) was purchased from TCI. Hydrochloric acid (37%−38% in water) was purchased from J. T. Baker. Tetramethylammonium chloride (TMACl, 97%) was purchased from Merck. All chemicals were used as received, except for divinylbenzene and styrene (>99%, Fluka), which were freshly distilled at 50 °C under vacuum to remove the inhibitors.

2.2. Synthesis. 2.2.1. (a) Synthesis and Functionalization of Fe_3O_4 Nanoparticles. Colloidal particles were prepared using a modification of the procedure originally described by Massart et al., based on the coprecipitation of Fe(II) and Fe(III) chlorides in basic solution. All steps were performed under argon. In a typical process 5.0 mmol of $FeCl_3 \cdot 6H_2O$ and 2.5 mmol of $FeCl_2 \cdot 4H_2O$ were dissolved in 10.0 mL of Millipore water (18.2 MΩ cm). This solution was injected dropwise into an aqueous solution of ammonium hydroxide (2 wt %) at 90 °C with vigorous mechanical stirring. After 30 min the formed black material was collected with a magnet to remove the supernatant. The stabilization of the iron oxide particles in aqueous media was then achieved by adding a mixture of 0.7 mmol of 16-heptadecenoic acid dissolved in 5.0 mL of an aqueous solution of ammonium hydroxide (2 wt %). After 1 h of stirring at 50 °C a stable dispersion containing Fe_3O_4 particles (9.0 nm ±2 nm) was received.

(24) Cayre, O.; Paunov, V. N.; Velev, O. D. *J. Mater. Chem.* **2003**, *13*, 2445.
(25) Fujimoto, K.; Nakahama, K.; Shidara, M.; Kawaguchi, H. *Langmuir* **1999**, *15*, 4630.
(26) Liu, B.; Wei, W.; Qu, X.; Yang, Z. *Angew. Chem., Int. Ed.* **2008**, *47*, 3973.
(27) Perro, A.; Reculusa, S.; Ravaine, S.; Bourgeat-Lami, E.; Duguet, E. *J. Mater. Chem.* **2005**, *15*, 3745.
(28) Perro, A.; Meunier, F.; Schmitt, V.; Ravaine, S. *Colloids Surf. A* **2009**, *332*, 57.
(29) Petit, L.; Sellier, E.; Duguet, E.; Ravaine, S.; Mingotaud, C. *J. Mater. Chem.* **2000**, *10*, 253.
(30) Pradhan., S.; Xu, L.-P.; Chen, S. *Adv. Funct. Mater.* **2007**, *17*, 2385.
(31) Perro, A.; Reculusa, S.; Pereira, F.; Delville, M.-H.; Mingotaud, C.; Duguet, E.; Bourgeat-Lami, E.; Ravaine, S. *Chem. Commun.* **2005**, *44*, 5542.
(32) Reculusa, S.; Poncet-Legrand, C.; Ravaine, S.; Mingotaud, C.; Duguet, E.; Bourgeat-Lami, E. *Chem. Mater.* **2002**, *14*, 2354.
(33) Reculusa, S.; Poncet-Legrand, C.; Perro, A.; Duguet, E.; Mingotaud, C.; Bourgeat-Lami, E.; Ravaine, S. *Chem. Mater.* **2005**, *17*, 3338.
(34) Lattuada, M.; Hatton, T. A. *J. Am. Chem. Soc.* **2007**, *129*, 12878.
(35) Isojima, T.; Lattuada, M.; Vander Sande, J. B.; Hatton, T. A. *ACS Nano* **2008**, *2*, 1799.
(36) Zhao, N.; Gao, M. *Adv. Mater.* **2009**, *21*, 184.
(37) Mirviss, S. B. *J. Org. Chem.* **1989**, *54*, 1949.

Scheme 1. Illustration of the Synthesis Procedure for Mushroom Nanostructures

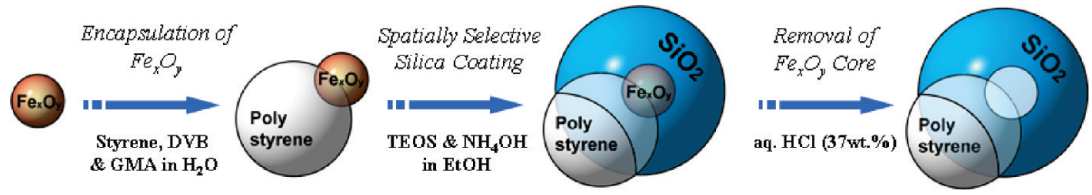

2.2.1. (b) Synthesis and Functionalization of α-Fe_2O_3 Nanoparticles. For the preparation of α-Fe_2O_3 nanoparticles 2 mmol of $FeCl_3 \cdot 6H_2O$ and 2 mmol of L-lysine were dissolved in 100 mL of Millipore water.[38] The solution was heated to 175 °C in an autoclave with a total volume of 110 cm^3. The size of the α-Fe_2O_3 crystals was controlled by the heating time (see Figure S1 and Table S1 in the Supporting Information). For example, to prepare 47.3 (±9.1) nm sized particles, the autoclave was cooled after 55 min reaction time. The resultant colloids were centrifuged (14 000 rpm, 12 min) and washed three times with water. Between washing and centrifugation, the colloid was redispersed by ultrasonication. To functionalize the iron oxide surfaces, 100 mg of α-Fe_2O_3 nanoparticles was dispersed in 15 mL of ammonia solution (1.3% NH_3 in water) containing 0.445 mmol of 16-heptadecenoic acid followed by ultrasonication for 0.5 h at 50 °C.

2.2.2. (a) Synthesis of Janus Fe_3O_4@PSD Nanospheres. For the synthesis of Fe_3O_4@DVB-2 colloids, 100 mg of the colloids produced by procedure 2.2.1a was stirred with 31.76 mmol of styrene, 0.67 mmol of DVB, and 2.32 mmol of glycidyl methacrylate (GMA) at 50 °C for 1 min. Then, 142 mL of warm ammonia solution (50 °C, 1.3 wt %) was added to the two-phase mixture. The black dispersion was quickly (within 10 min) heated to 70 °C. Once the solution reached 70 °C, 0.17 mmol of $(NH_4)_2S_2O_8$ dissolved in 2 mL of H_2O Millipore water was added with vigorous stirring to initiate the polymerization reaction. After 17 h, a stable gray dispersion was obtained. After three centrifugation and washing steps, PSD polymer immobilized Fe_3O_4 nanospheres were obtained. For the synthesis of Fe_3O_4@DVB-40 colloids, 17.67 mmol of styrene, 11.77 mmol of DVB, and 2.32 mmol of GMA were used as the monomer mixture in the same experimental setup. With this monomer composition, the morphology of the resulting composites can be controlled by the stirring period of the Fe_3O_4/monomer mixture. When the stirring period of the two phases was kept below 1 min, the magnetite particles were located at the surface of the polymer spheres (denoted Fe_3O_4@DVB-40a). When the mixture was stirred for at least 1 h, all Fe_3O_4 particles were found completely encapsulated inside the polymer spheres (denoted Fe_3O_4@DVB-40b). Fe_3O_4@DVB-100 colloids were synthesized with a monomer composition of 29.45 mmol of DVB and 2.32 mmol of GMA. Here, the magnetic particles were always completely encapsulated inside the polymer spheres: i.e., independent of the stirring period of the Fe_3O_4/monomer mixture.

2.2.2. (b) Synthesis of Janus Fe_2O_3@PSD Nanospheres. A 100 mg portion of the colloids produced by procedure 2.2.1b were partially encapsulated by the aforementioned cross-linked polymer (23.56 mmol of styrene, 5.89 mmol of DVB, and 2.32 mmol of GMA). After 1 h of moderate mechanical stirring at 50 °C, the reaction mixture was diluted with 142 mL of warm ammonia solution (1.3% NH_3 in water) and then heated to 70 °C and held at that temperature for 20 min. Subsequently, on addition of 0.17 mmol of $(NH_4)_2S_2O_8$ dissolved in 2 mL of H_2O, the polymerization reaction was allowed to proceed for 17 h with constant stirring at 70 °C. Afterward, the partially coated Fe_2O_3 nanoparticles (Fe_2O_3@PSD) were collected by centrifugation and washing three times as described above.

2.2.3. Controlled Growth of SiO_2 on Fe_xO_y@PSD Nanospheres. For asymmetric SiO_2 growth, 30 mg of the materials from 2.2.2a and 2.2.2b were diluted in 13.0 mL of ammonia solution (1.3% NH_3 in water) and stirred in 5 mL of ethanol for 1 h at room temperature. Then 20 mL of ethanol, premixed with a concentrated ammonia solution (0.81 mL 29% NH_3 in water), was added, followed by a direct addition of TEOS dissolved in ethanol (14.3 mL). The size of the SiO_2 moieties of the materials can be controlled by the amount of silica precursor (20, 60, or 300 μL). The solution was stirred for 16 h at room temperature. Finally, the received products were washed three times with ethanol by the procedure described above.

Alternatively, several surfactants (e.g., TMACl, TBABr, CTABr, and PVP-90) have been investigated for the controlled growth of silica. The synthetic procedure is essentially the same as that described above. The only difference is that instead of using 5 mL of ethanol, an ethanolic solution containing 0.09 mmol of surfactant and 5 mL of ethanol was used for the dissolution of 30 mg of the materials from 2.2.2a.

2.2.4. Hollow Derivatives of Fe_xO_y@PSD@SiO_2. A 30 mg portion of the mushroom nanostructures Fe_xO_y@PSD@SiO_2 was dispersed in 9 mL of concentrated HCl (37 wt %) and stored overnight. Afterward, the colloidal mushroom nanostructures were obtained by centrifugation and washing of acid-treated materials by the same procedure described in 2.2.2b.

2.3. Characterization. TEM and STEM analyses were carried out with Hitachi HF 7500 and Hitachi S-5500 microscopes, respectively. All samples were prepared on lacey carbon film supported by a copper grid. The IR spectra of samples were collected on a Magna-IR 750 Nicolet FTIR spectrometer using an ATR cell. XPS measurements were performed with a Kratos HSi spectrometer with a hemispherical analyzer. The monochromated Al Kα X-ray source ($E = 1486.6$ eV) was operated at 15 kV and 15 mA. For the narrow scans, an analyzer pass energy of 40 eV was applied. The hybrid mode was used as the lens mode. The base pressure during the experiment in the analysis chamber was 4×10^{-7} Pa. To account for charging effects, all spectra are referred to C 1s at 284.5 eV. Magnetic properties of the sample were measured using a superconducting quantum interference device (SQUID) magnetometer. N_2 sorption measurements were performed with a Micromeritics ASAP 2010 instrument.

3. Results and Discussion

3.1. Synthetic Strategy. Large-scale and easy synthesis of colloidal Janus nanoparticles by wet-chemistry approaches is a great challenge for modern science and technology. In this study, we have succeeded in the synthesis of Fe_xO_y@PSD−SiO_2 nanoparticles with spatially different functionalities, following the synthetic procedure illustrated in Scheme 1. In the first step, iron oxide nanoparticles were synthesized and dispersed in aqueous solution. In the second step, the iron oxide nanoparticles were immobilized (or encapsulated) in polymer via a radical emulsion-free polymerization to obtain monodisperse Fe_xO_y@PSD composite spheres. In the third step, the Fe_xO_y@PSD composite spheres obtained in the second step were spatially selectively coated with silica on one side of the spheres via a modified Stöber process,[39] thus forming the mushroom structures. Finally, if the mushroom structures with hollow interiors are more desirable, the obtained Fe_xO_y@PSD−SiO_2

(38) Wang, G.-H.; Li, W.-C.; Jia, K.-M.; Spliethoff, B.; Schüth, F.; Lu, A.-H. *Appl. Catal., A* **2009**, *364*, 42.

(39) Stober, W.; Fink, A.; Bohn, E. *J. Colloid Interface Sci.* **1968**, *26*, 62.

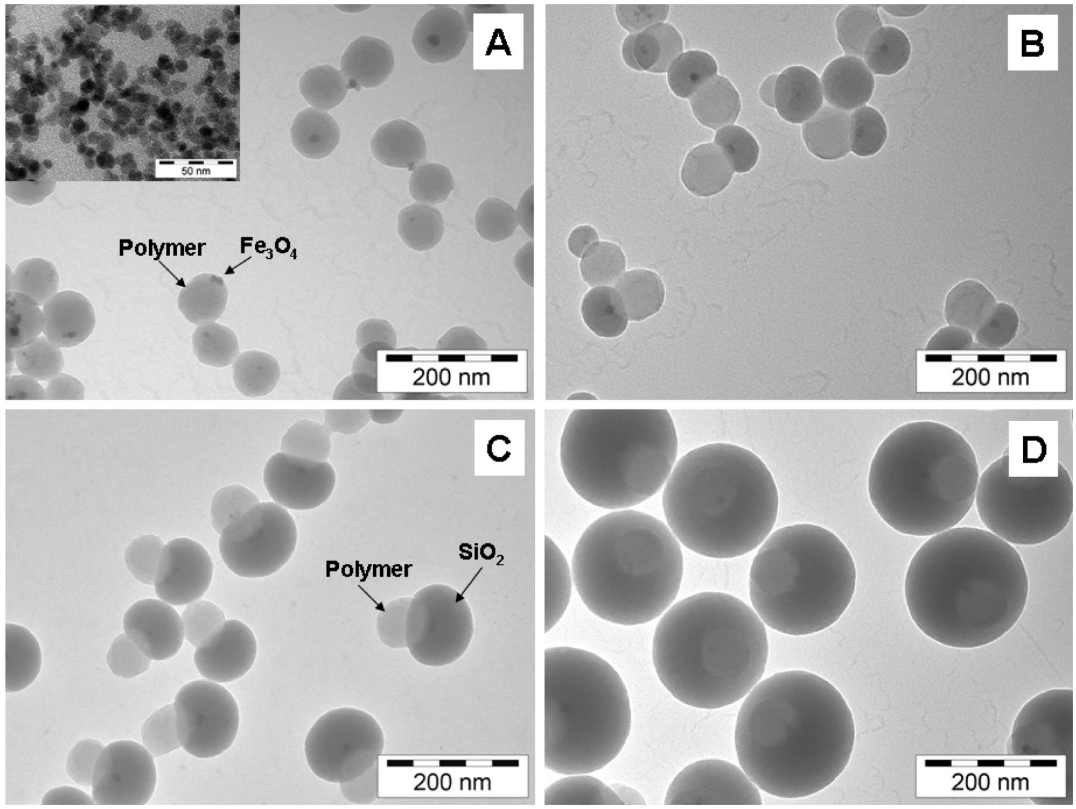

Figure 1. TEM images of Fe_3O_4@DVB-2 (A; the inset is the TEM of as-prepared Fe_3O_4 nanoparticles) and Fe_3O_4@DVB-2−SiO_2 (B−D). The average diameters of silica particles in B−D are 80, 110, and 180 nm, respectively.

from the third step can be treated with concentrated HCl aqueous solution. In order to elucidate the details of this synthetic mechanism, the products obtained from each step were carefully characterized by different techniques.

3.2. Mushroom Nanostructures of Fe_3O_4@PSD−SiO_2. TEM observation is a direct method for visualizing the structure of the product. TEM was thus used for the characterization of the products received from each step. As can be seen in the inset to Figure 1A, the synthesized magnetite nanoparticles have an average particle size of 9 ± 2 nm. After polymerization of poly(styrene-*co*-divinylbenzene) onto the iron oxide, uniform Fe_3O_4@DVB-2 spheres with a diameter of about 100 nm were obtained. As shown in Figure 1A, Fe_3O_4 nanoparticles (dark spots) were immobilized in the polymer matrix but located at or near the surface of one side of the polymer sphere. Using these Fe_3O_4@DVB-2 spheres as the seeds in a Stöber process for silica coating, mushroom nanostructures were obtained, as shown in Figure 1B−D. Obviously, the silica hemisphere is only growing on one side of the Fe_3O_4@DVB-2 spheres: i.e., it seems to nucleate at the Fe_3O_4. With an increasing amount of TEOS used, hemispherical silica particles with estimated sizes of 80, 110, and 180 nm (corresponding to Figure 1B−D) are grafted to one side of the Fe_3O_4@DVB-2 spheres. It is noteworthy that, even with relatively high amounts of TEOS, no full silica coating of the original particles was observed. Also, no random growth of silica particles on Fe_3O_4@DVB-2 seeds, which would lead to the formation of raspberry-like nanocomposites, was observed.[9] The synthesis was found to be very reproducible; batches were synthesized several times with virtually identical results (see Figure S2 in the Supporting Information). The synthesis was also scaled up by a factor of 20 and carried out in a 1 L flask. For example, starting with 30 mg of Fe_3O_4@HDA colloids, around 900 mg of Fe_3O_4@DVB-2−SiO_2 (silica size ca. 110 nm) could be recovered from one batch after centrifugation and washing steps. The obtained materials from the larger batch show shape and size identical with those prepared from a small batch (see Figure S3 in the Supporting Information). The formation of these particular mushroom nanostructures suggests that there is an anchor site directing the preferential growth of silica toward one direction. By close inspection of the interface between the polymer and the silica hemisphere, one can always clearly observe dark dots, corresponding to the Fe_3O_4 nanoparticles. Thus, we consider the Fe_3O_4 nanocrystals as anchor sites for silica growth which would actually be expected, since there would be OH groups on their surface, allowing facile interaction with the nucleating silica, as opposed to the rather hydrophobic PS-DVB surface of the polymer.

FT-IR spectroscopy was used to characterize the composition of these nanostructures (Figure 2A). The bands at 1525 and 1431 cm^{-1} in the spectrum for Fe_3O_4@HDA can be assigned to the bidentate interaction between the deprotonated carboxyl function of the HDA and the iron oxide surface.[40,41] Further, the presence of terminal vinyl groups in Fe_3O_4@HDA is revealed by the signals arising from stretching and deformation vibrations at 3088 and 910 cm^{-1}.

As seen in trace B of Figure 2 for the polymer composite Fe_3O_4@DVB-2, the four bands in the range 1450−1600 cm^{-1} clearly indicate the presence of benzene rings in this sample and, thus, the successful immobilization of Fe_3O_4 with PSD. With increasing size of the silica hemispheres in the silica-

(40) Rochiccioli-Deltcheff, C.; Franck, R.; Cabuil, V.; Massart, R. *J. Chem. Res.* **1987**, 1209.
(41) De Palma, R.; Peeters, S.; Van Bael, M. J.; Van den Rul, H.; Bonroy, K.; Laureyn, W.; Mullens, J.; Borghs, G.; Maes, G. *Chem. Mater.* **2007**, *19*, 1821.

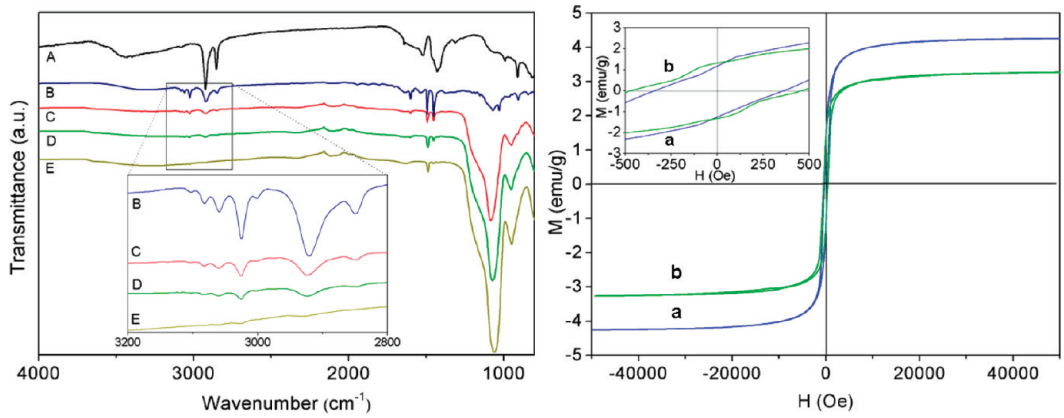

Figure 2. (left) ATR-IR spectra of Fe_3O_4@HDA (A), Fe_3O_4@DVB-2 (B), and Fe_3O_4@DVB-2@SiO_2 (C−E) nanoparticles with silica hemisphere sizes of 80, 110, and 180 nm, respectively. (right) M vs H curves of Fe_3O_4@DVB-2 (a) and Fe_3O_4@DVB-2−SiO_2 (b) measured at 10 K.

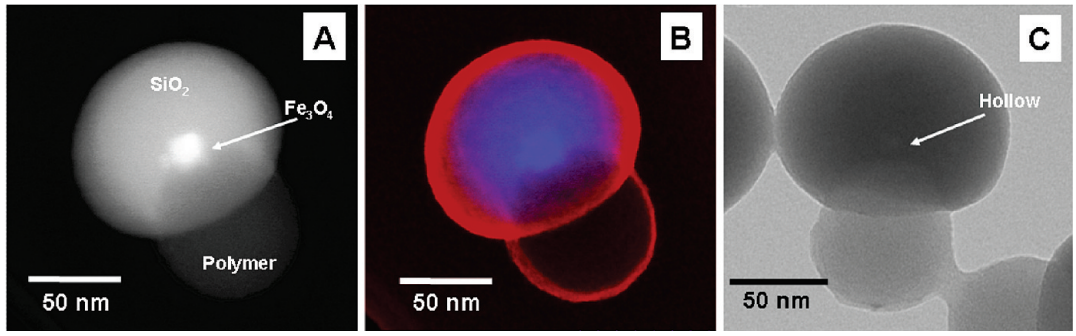

Figure 3. Dark field STEM image (A) and SEM and dark field STEM overlapping image (B) of Fe_3O_4@DVB-2−SiO_2 nanoparticles and TEM image (C) of Fe_3O_4@DVB-2−SiO_2 nanoparticles after HCl leaching.

modified samples (traces C−E in Figure 2), the relative intensities of the bands corresponding to ν(−C−H ar) 3057 cm^{-1}, ν(−CH_2−/−CH_3) 2924/2847 cm^{-1}, and ν(−C═C) 1602/1492/1450 cm^{-1} are decreasing, while the bands at 1100 and 950 cm^{-1}, corresponding to Si−O−Si and Si−OH stretching vibrations, become more significant, clearly indicating the presence of silica in the products.

Since the prepared mushroom nanostructures were (in the dried state) attractable by a conventional magnet, their magnetic properties were analyzed by SQUID. The recorded M vs H curves of Fe_3O_4@DVB-2 and Fe_3O_4@DVB-2−SiO_2 measured at 10 K are given on the right-hand side of Figure 2. Both curves show a sigmoidal curve with a small remanent magnetization (M_s) and coercivity (H_c) (M_s = 1.17/1.32 emu g^{-1} and H_c = 334/480 Oe for Fe_3O_4@DVB-2/Fe_3O_4@DVB-2−SiO_2, respectively) at low fields, which is typical for 10 nm sized magnetite particles below the blocking temperature.[42] The saturation magnetizations were estimated at 4.25 and 3.27 emu g^{-1} at a maximum field of 50 000 Oe, respectively. On normalization to the Fe_3O_4 content (5.5 wt % measured by TG) in Fe_3O_4@DVB-2, a saturation magnetization of 77.19 emu g^{-1} can be obtained. This value is in agreement with literature values for Fe_3O_4 and indicates that the magnetic properties of the Fe_3O_4 particles are maintained during processing.[43]

The detailed nanostructure of Fe_3O_4@DVB-2−SiO_2 nanoparticles was further characterized with high-resolution STEM. As displayed in Figure 3, one can clearly see that the Fe_3O_4 nanoparticles are located at the boundary between polymer and silica; the magnetite is completely enclosed by the silica coating.

As is known, iron oxide particles can be dissolved in concentrated HCl aqueous solution (37%). It should thus be possible to eliminate the Fe_3O_4 cores, if some porosity exists in the composites, thus creating a new hollow mushroom nanostructure. Fe_3O_4@DVB-2−SiO_2 colloidal particles were therefore treated with concentrated HCl (37%) aqueous solution, followed by centrifugation and washing with distilled water until the pH of the solution was close to 7. Indeed, the magnetic nanoparticles can be eliminated by acid solution, indicating that they are accessible through the silica and polymer shell.[44] Moreover, the shape was perfectly preserved after acid leaching and washing, reflecting the high stability of such nanostructures.

In order to better understand the formation mechanism of such mushroom nanostructures, the silica coating of Fe_3O_4@DVB-40a, Fe_3O_4@DVB-40b, and Fe_3O_4@DVB-100 spheres was also investigated. When Janus-type Fe_3O_4@DVB-40a nanoparticles (Figure 4A) were used as the seeds for silica growth, homogeneous mushroom nanostructures were obtained (Figure 4B). In contrast, if the completely polymer coated Fe_3O_4@DVB-40b and Fe_3O_4@DVB-100 nanoparticles were used as the seeds, silica particles were formed but not anchored on these seed particles (see Figure 4C−F). Separate silica particles and polymer-encapsulated magnetite particles were randomly mixed. Although occasionally silica particles attached to Fe_3O_4@DVB-40b could be found, the resulting nanostructures were not as homogeneous as those obtained by silica addition to Fe_3O_4@DVB-2−SiO_2. This clearly indicates that the position of the Fe_3O_4 in the cross-linked

(42) Batlle, X.; Labarta, A. *J. Phys. D* **2002**, *35*, R15.
(43) Caruntu, D.; Caruntu, G.; O'Connor, C. J. *J. Phys. D: Appl. Phys.* **2007**, *40*, 5801.
(44) Güttel, R.; Paul, M.; Schüth, F. *Chem. Commun.* **2010**, *46*, 895.

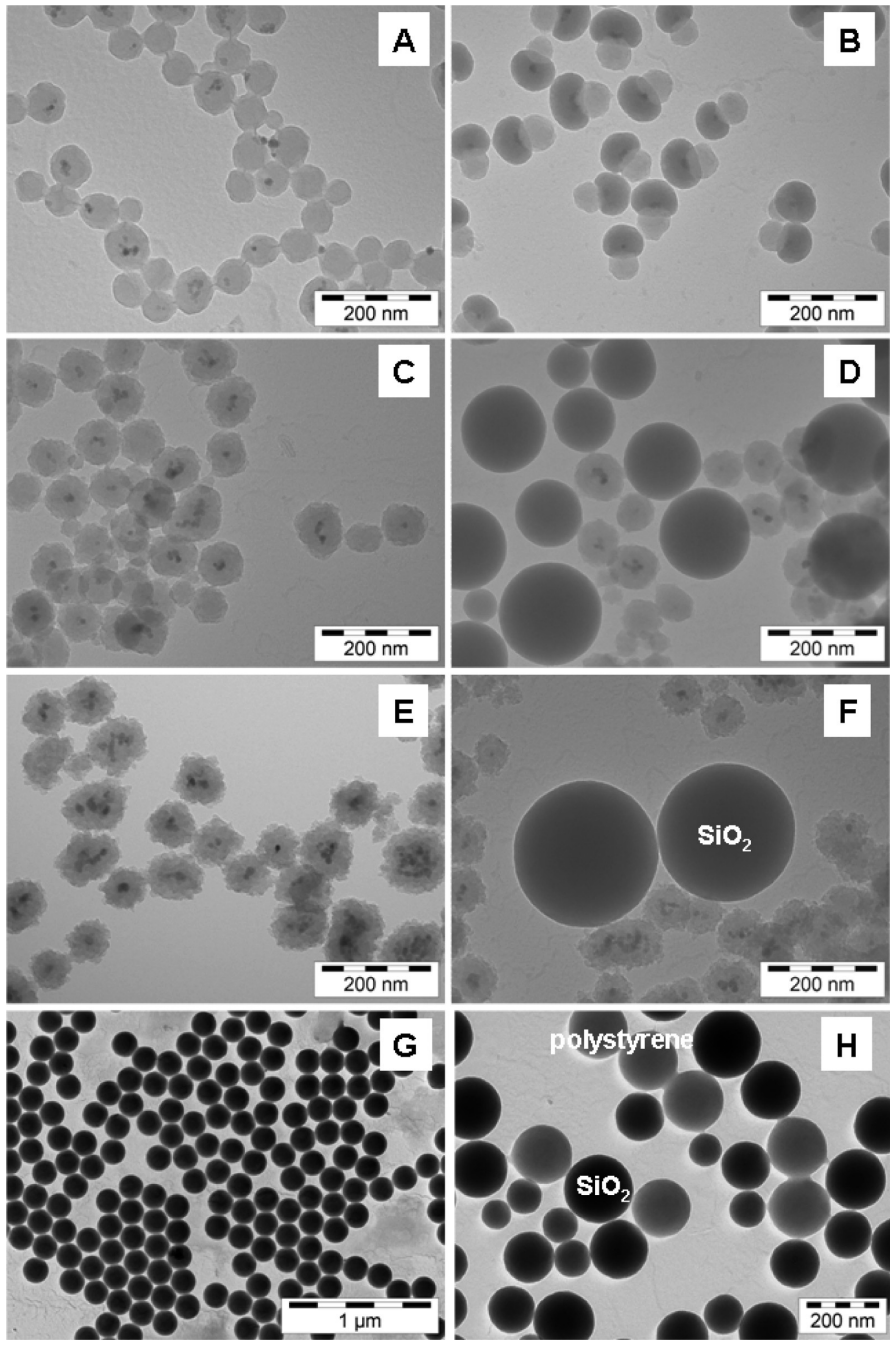

Figure 4. TEM images of Fe_3O_4@DVB-40a (A, B), Fe_3O_4@DVB-40b (C, D), Fe_3O_4@DVB-100 (E, F), and polystyrene particles (G, H) before (left) and after (right) silica coating.

polymer spheres is an important factor for the regioselectively controlled synthesis of such mushroom nanostructures.

For comparison, silica coating experiments were also performed in the absence of magnetite nanoparticles: i.e., pure polystyrene spheres prepared by the emulsion-free method with a diameter of about 170 nm were used as seeds for silica coating under the same experimental conditions used for Fe_3O_4@DVB-2. As seen in Figure 4 G,H, no mushroom nanostructures are observed. The dark and light particles, which correspond to silica and polystyrene, are not connected. This result demonstrates that no preferential growth of silica on the surfaces of the polystyrene spheres takes place in the absence of magnetite nanoparticles. A control experiment, in which Fe_3O_4 nanoparticles were directly coated with silica in the absence of the polymer under otherwise identical conditions, resulted in fully encapsulated Fe_3O_4 particles, in full agreement with previous literature data.[3,5,6] On the basis of these results, it is reasonable to conclude that the presence of Fe_3O_4 on/near the surface of the polymer particles is responsible for the seeded and localized growth of silica, so that the mushroom nanostructures form.

For additional insight into the formation mechanism of such nanostructures, the starting Fe_3O_4@DVB-x spheres with different amounts of DVB were analyzed by XPS (Figure 5). The surface compositions of these particles are summarized in Table 1. The majority of the oxygen is attributed to the incorporated HDA and GMA at the surface of the polymer spheres. The two types of oxygen species in all Fe_3O_4@DVB-x samples are correlated with the oxygen atoms in the carboxylic group of

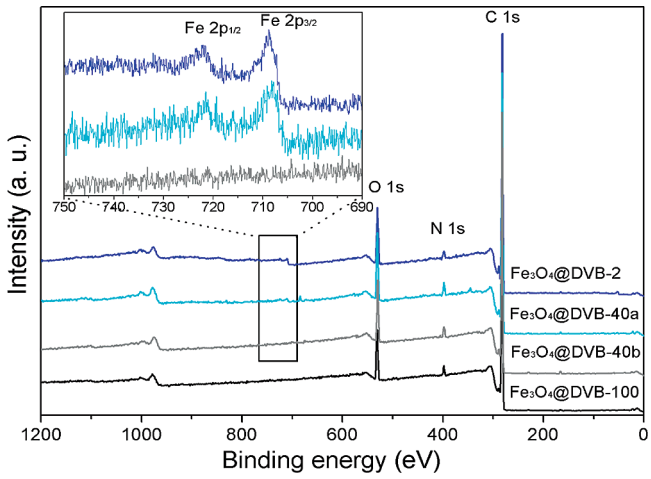

Figure 5. XPS of Fe_3O_4@DVB-2, Fe_3O_4@DVB-40a, Fe_3O_4@DVB-40b, and Fe_3O_4@DVB-100.

Table 1. Atomic Contents of the Surface Elements of Fe_3O_4@DVB-x Samples As Measured by XPS

sample	Fe (atom %)	C (atom %)	O (atom %)	N (atom %)
Fe_3O_4@DVB-2	detectable	89.0	9.0	2.0
Fe_3O_4@DVB-40a	detectable	80.0	14.4	5.0
Fe_3O_4@DVB-40b	not detectable	88.0	9.5	2.5
Fe_3O_4@DVB-100	not detectable	89.0	9.0	2.0

the HDA. Some small contribution to the oxygen signal may also come from the magnetite. Furthermore, all samples contain about 3% (atomic) of nitrogen, which could be ammonia ions immobilized on the spheres via reaction with the epoxy groups from the incorporated GMA molecules.

As can be seen in Figure 5 and Table 1, samples Fe_3O_4@DVB-2 and Fe_3O_4@DVB-40a show detectable amounts of iron. Judging from the intensity of the iron peaks, the content of iron in Fe_3O_4@DVB-2 is comparable to that of Fe_3O_4@DVB-40. Samples Fe_3O_4@DVB-40b and Fe_3O_4@DVB-100, prepared with an amount of DVB greater than 40 mol %, show no detectable iron species on their surfaces. Since the analysis depth of XPS ranges up to about 1−5 nm, depending on the material, the absence of any detectable iron signal for these two samples in the XPS analysis indicates that the magnetite nanoparticles are completely encapsulated by PSD. Photoelectrons generated from the iron particles cannot escape from the sample but are eliminated by the carbon shell. This is in agreement with the previous conclusion that no silica is attached to those seed spheres (Figure 4D).

3.3. Mushroom Nanostructures of Fe_2O_3@PSD−SiO_2. In order to examine whether the proposed growth mechanism of such mushroom nanostructures (shown in Scheme 1) is applicable to other iron oxides, hematite nanoparticles were chosen as alternative starting materials for the consecutive polymer and silica coating. Similar to the procedure shown in Scheme 1, hematite nanoparticles (Figure 6A) were first prepared using lysine as the modifier for their preparation (for the detailed synthetic procedure, see the Experimental Section). Subsequently, polymer encapsulation (2% of DVB was used) of hematite nanoparticles and further anisotropic silica growth steps were conducted under the same conditions as for Fe_3O_4@DVB-2. The samples obtained after each step were characterized by TEM and STEM. As can be seen in Figure 6B, after polymer encapsulation, discrete, polymer-encapsulated hematite nanoparticles were obtained. Careful TEM investigation reveals that the composite sphere exhibits an anisotropic structure: i.e., on

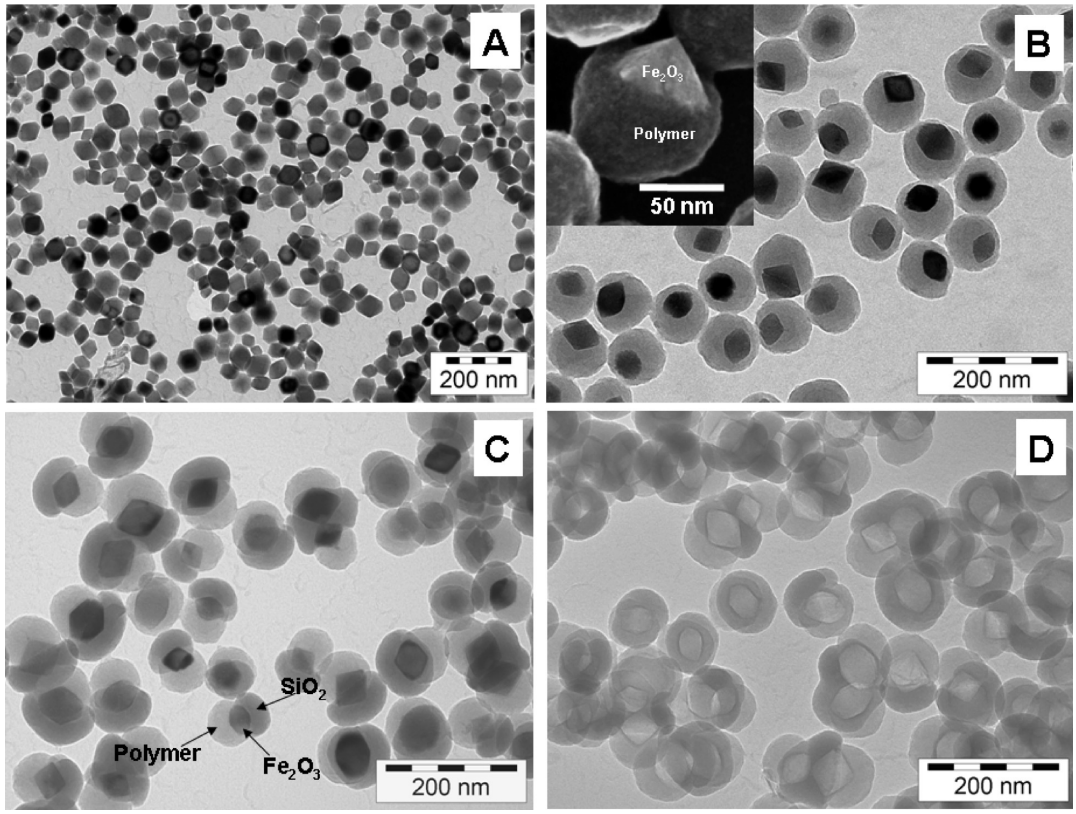

Figure 6. TEM images of Fe_2O_3 (A), Fe_2O_3@DVB-2 (B; the inset gives an SEM image), Fe_2O_3@DVB-2−SiO_2 (C), and the hollow derivative of Fe_2O_3@DVB-2−SiO_2 particles (D).

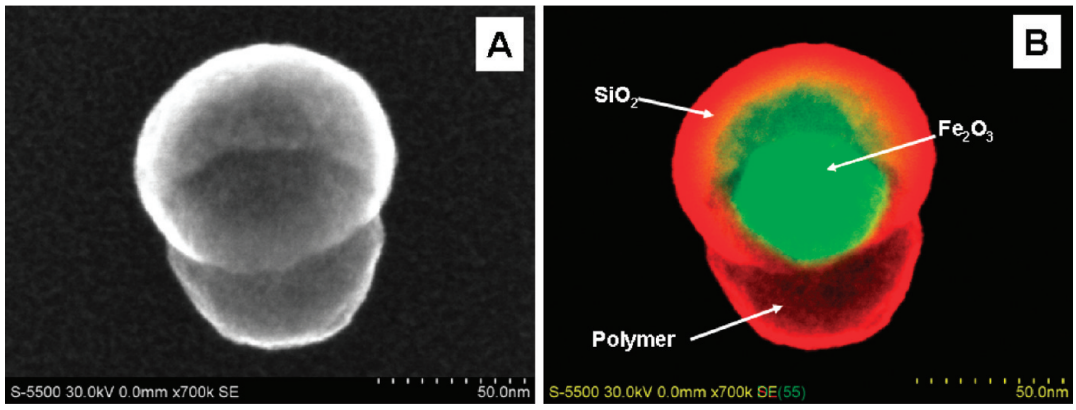

Figure 7. STEM image (A) and SEM and dark field STEM overlapping image (B) of Fe_2O_3@DVB-2−SiO_2 nanoparticles.

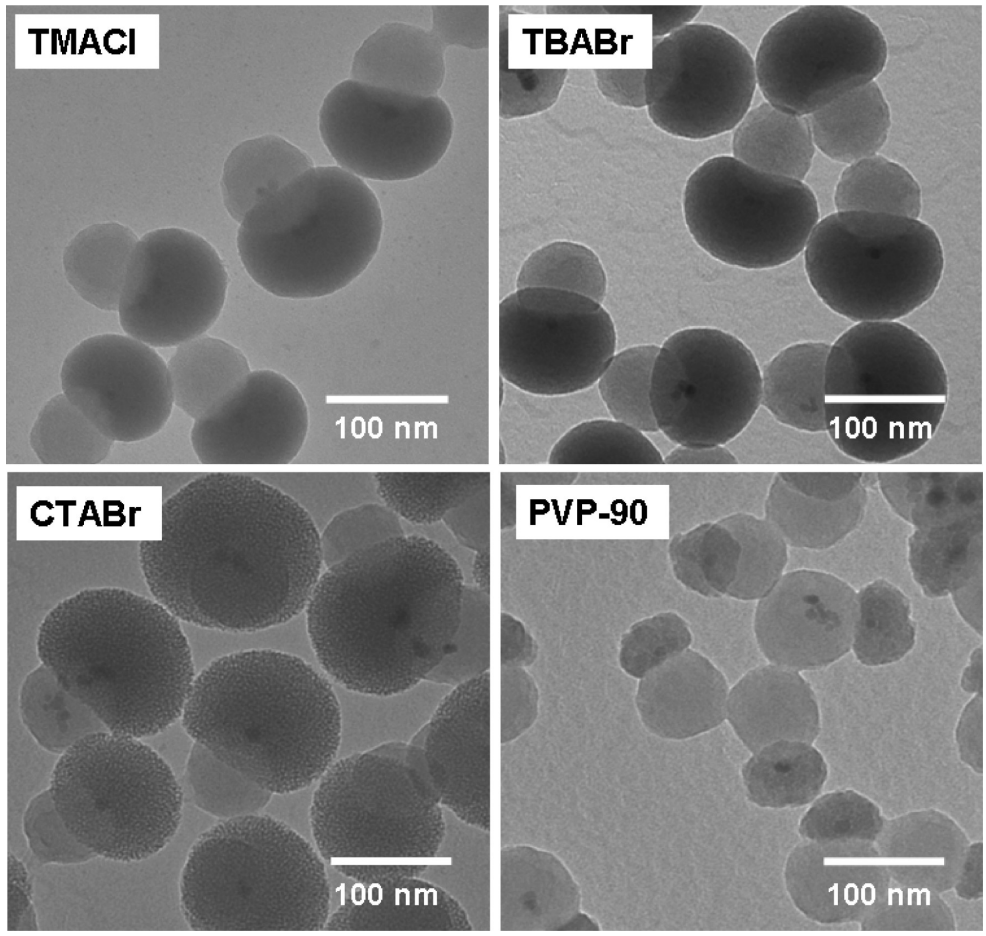

Figure 8. TEM images of mushroom nanostructures synthesized using different surfactants as porogens.

the one side of the composite sphere, the hematite nanoparticle is partially exposed, as displayed by high-resolution SEM observation (Figure 6B, inset). After the silica coating step, one can observe the mushroom nanostructures (Figure 6C). Silica nanoparticles indeed grew on the polymer/hematite particle, seeded by the exposed hematite nanocrystal. This experiment clearly confirms the growth mechanism of the anisotropic particles as illustrated in Scheme 1. These experiments demonstrate that, by the utilization of iron oxide nanocrystals as the anchor sites, mushroom nanostructures can willfully be synthesized by regioselective and directed decoration with silica. This provides opportunities for further engineering the silica or polymer surfaces via additional reactions.

Similar to Fe_3O_4@DVB-2−SiO_2 treated with concentrated HCl aqueous solution (37%), the hematite core of Fe_2O_3@DVB-2−SiO_2 is easily eliminated by acid solution. As seen in Figure 6D, mushroom nanostructures with a hollow interior are indeed formed, and they are structurally stable after this series of treatments. The morphologies of the hollow interiors are faithfully replicated from the shapes of the iron oxide nanoparticles. These hollow mushroom nanostructures might be interesting for the storage of molecules, for drug delivery, and as catalyst supports.

The detailed nanostructure of Fe_2O_3@DVB-2−SiO_2 was also carefully characterized with high-resolution STEM. As displayed in Figure 7A, the silica and polymer hemispheres are quite

smooth and no hematite is exposed on the outside, indicating that the hematite nanoparticles are well encapsulated. From Figure 7B, an overlapping image of SEM and dark field STEM, one can see clearly that the hematite nanoparticle is located exactly between polymer and silica. Again, STEM characterization on the Fe_2O_3@DVB-2−SiO_2 nanoparticles supports the proposed mechanism of regioselectively controlled synthesis of the mushroom nanostrucures. This mechanism might provide the blueprint for the synthesis of similar particles with different compositions.

3.4. Tuning the Mesoporosity of Fe_3O_4@PSD−SiO_2. Colloidal nanoparticles with tunable porosity instead of fixed values are more desirable for drug delivery, as adsorbents, or as catalyst supports. It is well-known that mesoporosity in silica effectively be created by using surfactants as porogens during the synthesis.[45,46] Hence, we examined the synthesis of such mushroom nanostructures in the presence of surfactants with the aim of creating mesopores in the silica hemisphere. As can be seen in Figure 8, also in systems where cationic surfactants (TMACl, TBABr, and CTABr) were added during the silica coating step, mushroom nanostructures were obtained in each case. By comparison with the results given in Figure 1, one can conclude that the presence of surfactant during the synthesis does not negatively affect the morphology of the products. In the case of the surfactant with small chain length (e.g., TMACl and TBABr), the obtained mushroom nanostructures (Figure 8, TMACl and TBABr) are quite similar to those synthesized without surfactant (Figure 1C). In contrast, using a cationic surfactant CTABr with longer chain length, mushroom nanostructures (Figure 8, CTABr) with visible mesoporosity were obtained. To further confirm the expected increase in surface area, nitrogen sorption measurements were performed on these mushroom nanostructures to estimate the pore parameters. Their surface area and pore volume are 316 $m^2\ g^{-1}$ and 0.19 $cm^3\ g^{-1}$, respectively. For comparison, the sample Fe_2O_3@DVB-2−SiO_2 prepared via the surfactant-free synthesis route was also characterized by the nitrogen sorption technique, and a surface area and pore volume of 41 $m^2\ g^{-1}$ and 0.08 $cm^3\ g^{-1}$, respectively, were determined. Hence, CTABr can indeed be used to create mesoporosity of such mushroom nanostructures. Notably, using PVP-90 as the surfactant, mushroom nanostructures with smaller silica moiety were obtained, as displayed in Figure 8. These results indicate that the fine structure of the mushroom nanostructures can be adjusted by the selection of proper surfactants which can be used to tailor the porosity and size of the silica moiety.

(45) Izutsu, H.; Mizukami, F.; Nair, P. K.; Kiyozumi, Y.; Maedab, K. *J. Mater. Chem.* **1997**, *7*, 767.
(46) Huo, Q.; Feng, J.; Schüth, F.; Stucky, G. D. *Chem. Mater.* **1997**, *9*, 14.

4. Conclusions

It was demonstrated that mushroom nanostructures (Fe_xO_y@PSD−SiO_2) and their hollow derivatives can be fabricated by consecutive immobilization (or partial encapsulation) of Fe_xO_y in polymer nanospheres and spatially controlled anchoring of silica with iron oxide as the nucleation site. It was found that the surface-accessible Fe_xO_y is the key for directing the growth of the silica hemisphere on Janus-type Fe_xO_y@PSD nanoparticles. The size and porosity of the silica hemispheres are tunable by adjusting the amount of TEOS used and by addition of proper surfactants in a Stöber process. After the iron oxide cores were leached out with concentrated HCl, mushroom nanostructures with hollow interiors were obtained. The morphology of the hollow interior faithfully replicates the shape of the iron oxide core. These mushroom nanostructures and their hollow derivatives could be very interesting building blocks for the assembly of other new types of nanostructures and as carriers for drug delivery, catalysis, or multifunctional sensoring.

Acknowledgment. A.-H.L. acknowledges the financial support of the NSFC (No. 20873014) and the Program for New Century Excellent Talents in University (NCET-09-0254), the Ministry of Education, P. R. China. We are grateful for the basic funding provided by Max-Planck-Institut für Kohlenforschung.

Supporting Information Available: TEM images of the reproduced and scaled up Fe_3O_4@DVB-2−SiO_2 and TEM images and a table including the synthetic parameters of Fe_2O_3 with different sizes. This material is available free of charge via the Internet at http://pubs.acs.org.

JA101270R